

Sgr A* at low radio frequencies: GMRT observations

Subhashis Roy* & A. Pramesh Rao†

National Centre for Radio Astrophysics (TIFR),

Pune University Campus, Post Bag No.3, Ganeshkhind, Pune 411 007, India

ABSTRACT

The central region of the Galaxy has been observed at 580, 620 and 1010 MHz with the Giant Metrewave Radio Telescope (GMRT). We detect emission from Sgr A*, the compact object at the dynamical centre of the Galaxy, and estimate its flux density at 620 MHz to be 0.5 ± 0.1 Jy. This is the first detection of Sgr A* below 1 GHz (Roy & Rao 2002, 2003), which along with a possible detection at 330 MHz (Nord et al. 2004) provides its spectrum below 1 GHz. Comparison of the 620 MHz map with maps made at other frequencies indicates that most parts of the Sgr A West HII region have optical depth ~ 2 . However, Sgr A*, which is seen in the same region in projection, shows a slightly inverted spectral index between 1010 MHz and 620 MHz. This is consistent with its high frequency spectral index, and indicates that Sgr A* is located in front of the Sgr A West complex, and rules out any low frequency turnover around 1 GHz, as suggested by Davies et al. (1976).

Key words: Galaxy: centre – ISM: HII regions – techniques: interferometric.

1 INTRODUCTION

Being located two orders of magnitude closer than the nearest large galaxy, the Galactic Centre (GC) can be studied at a much higher spatial resolution and sensitivity than is possible for other galaxies. Because of this advantage, we can identify unique objects like the Radio-arc consisting of linear parallel filaments (Yusef-Zadeh et al. 1984), or the $2.6 \times 10^6 M_{\odot}$ black hole suggested to be associated with the compact radio source Sgr A* (Ghez et al. 1998). From the high resolution (\sim arc seconds) observation by the Very Large Array (VLA) at radio frequencies (Ekers et al. 1983; Pedlar et al. 1989), the following sources within the central $15'$ of the Galaxy have been identified.

(i) At the dynamical centre of the Galaxy is the compact nonthermal radio source known as Sgr-A*. (ii) Around Sgr A* is the HII region Sgr-A West (Ekers et al. 1983), whose morphology resembles a face-on spiral galaxy. (iii) Near Sgr-A West is Sgr-A East, which is believed to be a supernova remnant (SNR). (iv) A $7'$ halo, which has been proposed to be a mixture of thermal and non-thermal emission (Pedlar et al. 1989).

Sgr A* (see Melia & Falcke 2001 for a review) was not detected at frequencies below 960 MHz and observations at 408 MHz (Davies et al. 1976) and at 330 MHz (Pedlar et al. 1989) provide upper limits (≤ 0.1 Jy at 330 MHz) on its flux density. Sgr A* probably has a low frequency turnover below 1 GHz, but the nature of the turnover has never been examined in detail (Melia & Falcke 2001). Recently, Nord et al. (2004) claim to have detected Sgr A* at 330 MHz. However, the average brightness of the $7'$ halo seen

towards Sgr A* at 330 MHz is ~ 100 mJy/Beam (with the beam-size used in their map), which is comparable to the claimed peak intensity of Sgr A* (Fig. 2 in Nord et al. 2004). The $7'$ halo could be located in front of the Sgr A complex (Pedlar et al. 1989), and presence of any small scale structure in the halo along Sgr A* can mimic its claimed detection. Therefore, detection of Sgr A* at 330 MHz remains provisional.

High resolution radio observations (Roberts & Goss 1993) show that Sgr A West comprises of three major features of ionised gas known as Northern and Southern arm and Western arc, which are embedded in a halo of lower density ionised gas with an extent of about $1.5'$ (Mezger & Wink 1986; Pedlar et al. 1989). Along the Northern arm, the gas appears to flow away from us. If this is taken as an indication of gas falling in towards Sgr A*, then this would imply that the Northern arm is located in front of Sgr A*. Though Whiteoak et al. (1983) have suggested Sgr A* to be located in front of Sgr A West, Liszt et al. (1983) detected HI absorption against Sgr A* at $40\text{--}60 \text{ km s}^{-1}$, and not against Sgr A West. While Liszt et al. (1983) attributes this discrepancy to the patchiness of the HI screen, the relative location of Sgr A* with respect to Sgr A West need to be established.

Due to free-free absorption at low radio frequencies, HII regions tend to get optically thick and absorption against another continuum object can be used to constrain their relative location.

We have observed the central half a degree region of the Galaxy at 580, 620 and 1010 MHz using the GMRT (Swarup et al. 1991). As a cross-check, we have observed Sgr A* also at 580 MHz. To estimate its spectral index between 1 GHz and 620 MHz and compare with its spectrum obtained at higher radio frequencies, we have further observed this region at 1010 MHz with the GMRT.

* E-mail: roy@ncra.tifr.res.in

† E-mail: pramesh@ncra.tifr.res.in

In this paper, we will mainly discuss Sgr A* and Sgr A West HII region. In Sect. 2, we describe the observations and data analysis. The results are presented in Sect. 3, and the inferences are discussed in Sect. 4. The conclusions are presented in Sect. 5.

2 OBSERVATIONS AND DATA REDUCTION

The observations were carried out with the Giant Metrewave Radio Telescope (GMRT) with a nominal bandwidth of 16 MHz on Aug 31 & Sept 21, 2001 at 620 MHz and in June 2002 at 580 MHz. Full synthesis (~ 7 hours) was performed at these frequencies. The field centre was set at RA (J2000)=17h46m07s, DEC (J2000)=-28°57'02". The observations in the 1010 MHz band were carried out on 9th of August 2003. These were (1010 MHz) two snapshot observations each of about 45 minutes in duration, and the field centre was set at RA (J2000)=17h45m40.5s, DEC (J2000)=-28°56'09". All these observations were carried out in the spectral line mode with 128 frequency channels across 16 MHz. Absolute flux density calibration was performed using 3C48 and 3C286 data following Baars et al. (1977) scale. The source 1751–253 and 1714–25 were used as secondary and bandpass calibrator respectively. At 1010 MHz, 3C286 was used for bandpass calibration.

The increase of T_{sys} from the calibrator field to the target source affects the source visibility amplitudes in the default observing mode (i.e., the Automatic Level Control (ALC) in the system is turned on), and we employed the following method to correct for the T_{sys} variation. With the ALC off, we estimated the ratio of the total power on the target source and the calibrator 3C48 at 620 MHz. Since this ratio was quite similar (within 10%) for almost all the antennas, rather than multiplying the antenna based gain, we multiplied the final map of the source intensity distribution by this number.

The ALCs are employed to keep the input power to the correlator constant, which in turn keeps the effective gain of the correlator constant. However, our tests show that a variation in input power by a factor of 4 changes the effective gain of the 4-bit correlator by $\leq 5\%$. Since the variation in total output power between the GC and the secondary calibrator with the ALC off is also ~ 4 , to prevent T_{sys} affecting directly the visibility amplitudes, the ALCs were turned off for 580 MHz and 1010 MHz observations, which were carried out after the 620 MHz observations. The absolute flux density scale using the first method (i.e., at 620 MHz) is believed to be accurate to about 10%, while, it is expected to be accurate to better than 5% with ALCs off (i.e., at 580 and 1010 MHz).

The data were processed within the Astronomical Image Processing System (AIPS) using standard programs. Bad data were identified and flagged using various tasks in AIPS. After calibration and editing of the 620 MHz data, a pseudo-continuum database of 3 frequency channels (each of width 3.7 MHz) was made from the central 11 MHz of the observed 16 MHz band. This was adequate to avoid bandwidth smearing within the primary beam. Images of the fields were formed by Fourier inversion and Cleaning (IMAGR). The initial images were improved by phase only self-calibration (Self-cal). However, subsequent amplitude and phase Self-cals failed to improve the dynamic range of the maps. Therefore, phase only Self-cals were used to produce the final images.

To improve the deconvolution of the extended emission, we made the final image (Fig. 1) using Multi-resolution Clean (Wakker & Schwarz 1988) as implemented in AIPS. Since the strong emission is seen mostly near the central 10' region of the

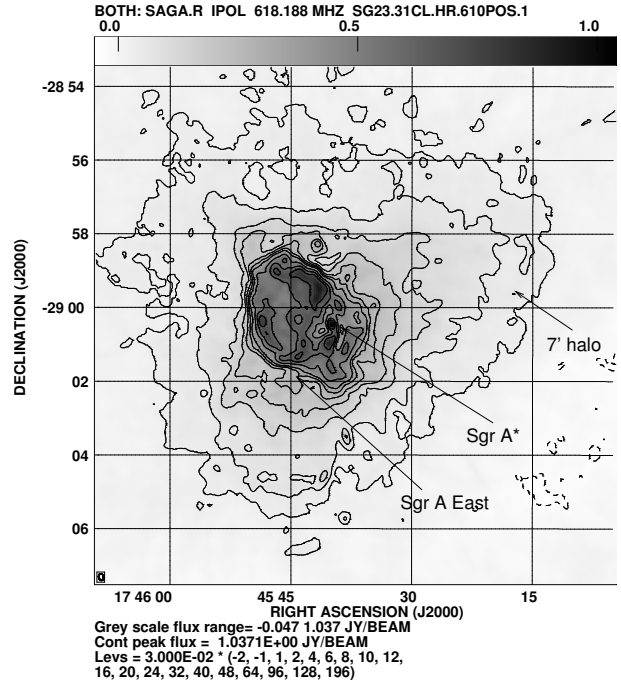


Figure 1. 620 MHz GMRT map of the central 15' region of the Galaxy (in both contour and gray scale). The resolution is $11.4'' \times 7.6''$, with beam position angle of 7.7° . The rms noise is about 6.5 mJy/Beam.

GC, and we are interested in sources located within only this region, no 3D deconvolution of the dirty image to compensate for the non-coplanar baseline effect was performed. The GMRT map at 620 MHz (Fig. 1) has a dynamic range of about 150, and is limited by systematics. The above procedures were also employed to calibrate the 580 MHz and 1010 MHz data, and to make images at 580 MHz. Phase only Self-cals were performed with the Clean Components of Sgr A* at 1010 MHz to produce the final self-calibrated uv -data.

3 RESULTS

3.1 Features in the 620 MHz map

The central 15' region of the Galaxy at 620 MHz is shown in Fig. 1. The compact source Sgr A* is clearly seen, along with other well known sources like Sgr A East and the 7' halo, which were also seen in our earlier 610 MHz map (Roy & Rao 2002), but due to change in calibration scheme and in subtraction of the background extended emission (see Sect. 3.2.1), the earlier results from Roy & Rao (2002) will not be used in drawing any quantitative estimation in this paper.

To compare the smaller scale features near Sgr A West with what is seen at higher frequencies, we have plotted in Fig. 2, the 620 MHz map in gray scale and the 4.8 GHz VLA map in contours convolved to a common resolution. There is almost one to one correspondence between the higher emission features at 4.8 GHz comprising the Sgr A West region and a drop in the total intensity at 620 MHz (indicated by white region in the gray scale map), indicating that the thermal emission is optically thick near 620 MHz. The shell-like emission feature known as Sgr A East is clearly identified in both the maps. An emission feature $\approx 30''$ south of Sgr A* can be seen in the 620 MHz gray scale map. This

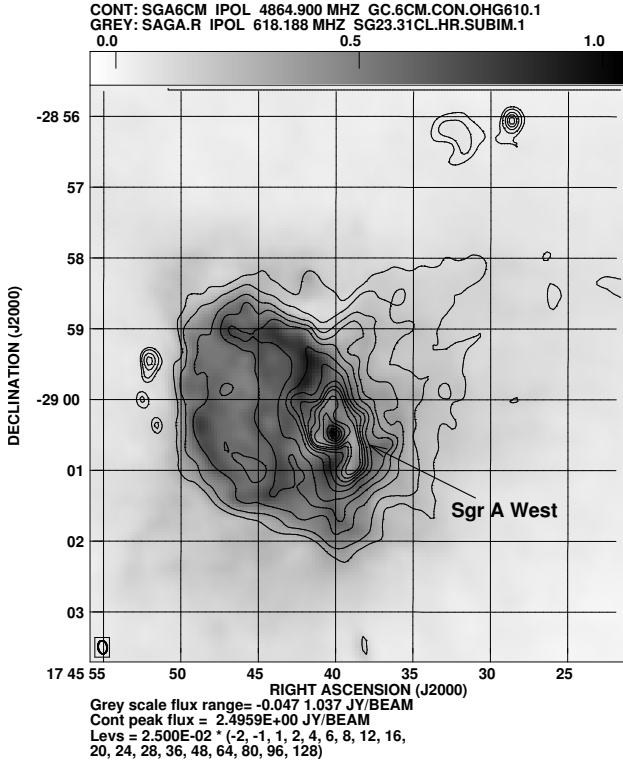


Figure 2. 4.8 GHz continuum map of the Sgr A complex (Yusef-Zadeh 1989) in contour overlaid on the 620 MHz gray scale map of the same region. The resolution is $11.4'' \times 7.6''$, with beam position angle of 7.7° . The rms noise in the 4.8 GHz map is about 4 mJy/Beam.

feature was identified by Pedlar et al. (1989), who suggested that it is associated with Sgr A East. The Sgr A East shell has a size of about $2' \times 3'$, and there is a triangular shaped halo of size $\sim 7'$ around its shell, which is known as the $7'$ halo.

3.2 Emission measure and temperature of the ionised gas in the Sgr A West HII region

In this section, we estimate the density and temperature of ionised hydrogen in Sgr A West. Pedlar et al. (1989) estimated these parameters by assuming a constant electron temperature across Sgr A West. However, due to the availability of high resolution data at 4 different frequencies between 8.3 GHz and 620 GHz, we can study the variation of the electron temperature (T_e), the emission measure ($\int n_e^2 dL$, where L is the path length through the ionised medium) and the background non-thermal flux density due to Sgr A East as functions of position in the map. To estimate the quantities, the optical depth of the Sgr A West HII region as a function of frequency needs to be estimated, which we describe below.

While estimating flux densities from different maps, the synthesised beam of each of the maps needs to be equal. We have convolved the 8.3 GHz, 4.8 GHz, 1.4 GHz and 620 MHz maps to a common resolution of $11.4'' \times 7.6''$, with beam position angle of 7.7° . In Fig. 1, there are four sources, Sgr A*, Sgr A West, Sgr A East and the $7'$ halo, which appear to overlap along the line of sight. Because of this overlap, estimating flux densities of Sgr A West is non-trivial. Based on the suggestion of Pedlar et al. (1989), we assume that the $7'$ halo is located in front of the Sgr A complex. We took crosscuts at several orientations across the $7'$ halo through the location of Sgr A*, and estimated its mean contri-

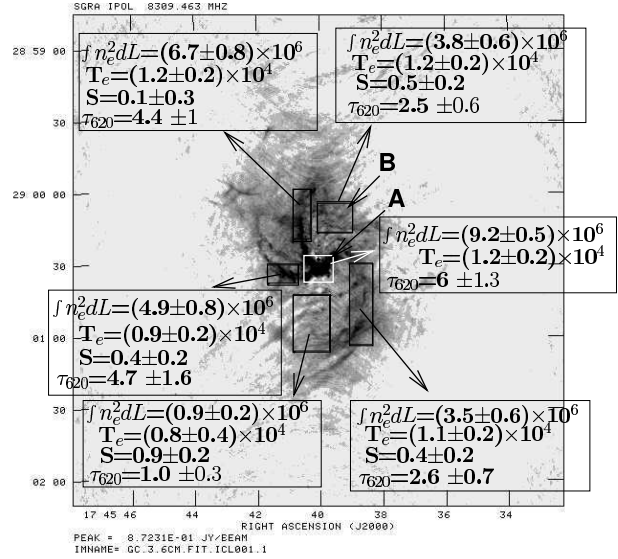


Figure 3. Estimated electron temperature, emission measure (in boxes) and average optical depth at 620 MHz (τ_{620}) at 6 different parts of Sgr A West. These parts are enclosed in rectangular boxes drawn on the 8.3 GHz gray scale map (Roberts & Goss 1993)

bution across the Sgr A complex. The estimated intensity of the $7'$ halo is 0.18 Jy/Beam at 620 MHz and at 1.4 GHz. The background emission due to $7'$ halo is quite small at 4.8 GHz, where it gets partially resolved due to the lack of short interferometric spacings, and we estimate its contribution at this frequency to be about 0.012 Jy/Beam (no background subtraction was performed at 8.3 GHz). After subtracting these intensities of the $7'$ halo from the corresponding maps, the flux densities at different parts of Sgr A West were estimated. Even if the $7'$ halo is considered to be a mixture of thermal and non-thermal emission (Pedlar et al. 1989), from the estimates made by Pedlar et al. (1989) at 330 MHz, it can be considered to be optically thin at frequencies of 620 MHz and above. Consequently, after subtraction of emission from the $7'$ halo and the removal of the contribution from Sgr A*, the observed flux density towards Sgr A West is the sum of non-thermal emission from Sgr A East (located behind Sgr A West (Pedlar et al. 1989)) and its own thermal emission. The observed flux density from Sgr A East can be expressed as $S\nu^\alpha \times \exp(-\tau)$, where S is the flux density of the background source at 1 GHz in Jy/Beam, τ is the free-free optical depth at a frequency of ν GHz and α is the spectral index. The estimated flux density due to free-free emission is $[2kT_e \times (1 - \exp(-\tau)) \times \nu^2 \times \Delta\Omega]/c^2$. Where, $\Delta\Omega$ is the synthesised beam size. From the radiative transfer equation, we can express the estimated flux density per synthesised beam as

$$I_\nu = S\nu^\alpha \times \exp(-\tau) + [2kT_e \times (1 - \exp(-\tau)) \times \nu^2 \times \Delta\Omega]/c^2. (1)$$

$$\text{Where, } \tau = \int 0.2n_e^2 T_e^{-1.35} \nu^{-2.1} dL.$$

Following Pedlar et al. (1989), we assume the spectral index of Sgr A East to be -1.0 ($S(\nu) \propto \nu^\alpha$) between 8.3 GHz and 620 MHz. The average intensity per synthesised beam estimated at different frequencies from each of 4 different regions corresponding to the Western arc, Northern and Southern arm, and the diffuse halo (sampled at two different parts) as shown in Fig. 3, were least square fitted with the expression for I_ν given above. The estimated T_e and $\int n_e^2 dL$ and the optical depth at 620 MHz (τ_{620}) for these regions are also shown in Fig. 3. We note that the estimated parameters do not vary significantly, even if the spectral index of Sgr A

East changes from -1.0 by ± 0.5 between 1.0 GHz and 620 MHz. Sgr A* is seen through the region marked 'A', and we subtracted its observed flux density at the position of Sgr A* (see below) from each of the different frequency maps. The fit of intensities of region 'A' to the expression for I_ν did not converge, and 'S' was held fixed to zero to get a fit (see Fig. 3). Since there is no measurable increase in the flux density from this region between 8.3 and 4.8 GHz (thermal emission is optically thin at these frequencies), the non-thermal emission from Sgr A East is negligible, and therefore keeping S fixed to 'zero' should have negligible effect on the estimated parameters.

From the model fit to all of the above mentioned regions, the electron temperature is found to be within 8,000–12,000 K, which is higher than the reported value of 7000 K by recombination line observation of Roberts & Goss (1993). They assumed the emitting gas to be in local thermodynamic equilibrium (LTE), and that pressure broadening is negligible. However, the estimate of T_e from the continuum spectrum, anchored at the low frequencies by the GMRT measurements, is free from any such assumptions and provide a more accurate value.

3.2.1 Flux density of Sgr A*

While estimating the flux density of Sgr A* at 620 MHz, we reduced the confusion due to the extended emission by imaging only those visibilities having uv distance $> 7 k\lambda$. The flux density estimated from the image plane is about 0.5 ± 0.1 Jy. We note that even after applying a lower uv cutoff, there is significant background confusion within a beam of size $7.5'' \times 4''$. This confusion causes an uncertainty of about 0.1 Jy in the estimated flux density. We also estimated the flux density of this object from the uv visibilities. We first applied appropriate phase shift such that Sgr A* is at the phase centre. Every one hour of uv -data were averaged vectorially, which ensures that the sources away from the centre have little contribution to the visibility amplitude. After rejecting data with uv -distance shorter than $15 k\lambda$, an elliptical Gaussian model was fitted as a model for Sgr A* (using UVFIT). The flux density estimated in this way is also 0.5 Jy. The major and minor axis of the Gaussian fit is $3.8'' \pm 0.4''$ and $1.8'' \pm 0.6''$ respectively with a position angle of $93 \pm 4^\circ$, which is consistent with its expected scatter broadened size of $3.4'' \times 1.8''$ estimated from Lo et al. (1998) at this frequency. To check the goodness of the fit, we divided the uv -data by the model. Similar broadening of compact maser sources in the vicinity of OH/IR stars have been observed in the central 30' of the Galaxy (van Langevelde et al. 1992). The real part of the data after division indeed is close to unity with a scatter of less than 0.2, which indicates an rms error of 0.1 Jy in the flux density measurement.

We also imaged Sgr A* from the 580 MHz data. The flux density estimated at this frequency matches (within the error-bar) to what is estimated at 620 MHz and its known spectrum at radio frequencies. The flux density of Sgr A* at 1010 MHz as estimated from the uv visibilities is 0.6 ± 0.12 Jy.

4 DISCUSSION

4.1 Low frequency spectral index of the Sgr A*

Although the high radio frequency spectrum of Sgr A* is well established, the spectrum below 1.4 GHz is not well estimated. At 1010 MHz, the flux density of Sgr A* is about 0.6 Jy and its

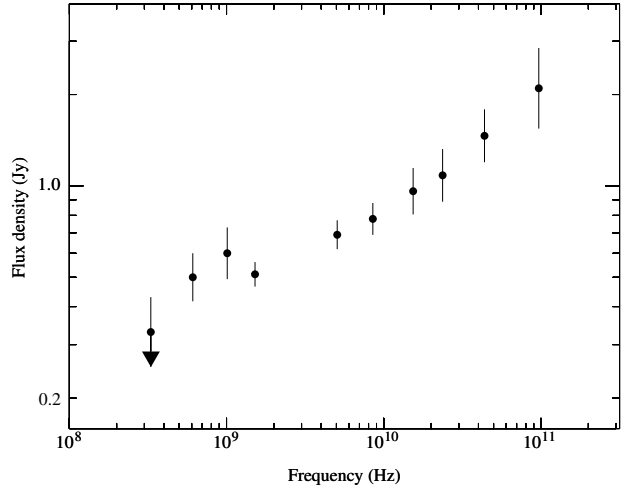


Figure 4. The observed spectrum of Sgr A* from 300 MHz to 20 GHz. Except the 330, 620 and 1010 MHz measurements, all the other data points are taken from Melia & Falcke (2001). In the plot, the 330 MHz flux density estimated at the position of Sgr A* (Nord et al. 2004) is taken as the upper limit.

time averaged spectral index between 1.4 and 8.5 GHz is $+0.17$ (Melia & Falcke 2001). Davies et al. (1976) found the flux density of Sgr A* at 960 MHz to be a factor of 2 less than at 1.6 GHz and suggested that it has a low frequency turnover around 1 GHz. This appears to be confirmed from their upper limit of 50 mJy at 408 MHz and the 100 mJy upper limit set by Pedlar et al. (1989) at 330 MHz. However, Nord et al. (2004) at 330 MHz estimate a total flux density of 330 ± 120 mJy from the known position and expected size of Sgr A*. The recent flux density estimates of Sgr A* at 1010, 620 and 330 MHz raises questions about earlier measurements. Based on the average flux density of Sgr A* at 1.4 GHz (Zhao et al. 2001) and its known spectrum between 1.4 and 8.5 GHz, we expect a flux density of 0.47 Jy at 1010 MHz and 0.44 Jy at 620 MHz, which are consistent with our measurements within the error-bars. The observed spectrum of Sgr A* from 300 MHz to 20 GHz is shown in Fig. 4. From the spectrum it is apparent that a factor of two lower flux density at 960 MHz (Davies et al. 1976) can be explained only by assuming Sgr A* to be variable at this frequency. Falcke (1999) finds a modulation index of 6% at 8.3 and 2.5% at 2.3 GHz, which indicates that the intrinsic variability of Sgr A* is rather low at low radio frequencies (Melia & Falcke 2001). Therefore, interstellar scintillation (ISS), the time scale of which is \sim few years towards Sgr A* at 1 GHz, is likely to cause any significant variability. The observations in the 620 MHz band cover a span of nearly an year and no significant variation ($\sim 20\%$) could be detected. Our measurements rule out any turnover near 1 GHz and indicate that any turnover has to be at frequencies less than 580 MHz. The upper limits at 408 MHz, however, pose problems for this picture, as this would suggest the flux density of Sgr A* at this frequency could have been much less few decades back. We have re-examined the 408 MHz upper limit by Davies et al. (1976) and found that their analysis has not taken account of scatter broadening of Sgr A* (about $8''$ at 408 MHz) and the corrected upper limit at 408 MHz could be as high as ≈ 2.5 Jy.

At frequencies of a few GHz to 620 MHz, the observed spectral index of Sgr A* is nearly flat. For extragalactic flat spectrum sources, it is believed that there are multiple components in emission and peak radiation from different components occur at different frequencies to make the overall spectrum appear nearly

flat (Cotton et al. 1980). Though the Advection-dominated accretion flow (ADAF) model of emission from Sgr A* fails to explain the observed low frequency emission, ADAF along with self-absorbed synchrotron emission either from a relativistic Jet (Yuan et al. 2002), or from a small fraction of relativistic electrons embedded in the accretion flow (Yuan et al. 2003) could explain the observed spectrum of Sgr A* from X-ray ranges to radio frequencies up to 620 MHz. If we consider the flux density estimated at the position of Sgr A* at 330 MHz (Nord et al. 2004) as the observed upper limit, its estimated spectral index between 620 and 330 MHz is inverted and is >0.66 . This low frequency turnover could be due to an enhancement in the optical depth of synchrotron emission or internal/external free-free absorption.

4.2 Location of Sgr A*

At 620 MHz, Sgr A West shows evidence for free-free self-absorption. In Fig. 3, we have shown the mean optical depth for 6 different regions of Sgr A West. The Sgr A* being slightly above the junction of the Bar and the Northern arm (Roberts & Goss 1993), optical depth near Sgr A* is almost the same as the Sgr A West halo marked 'B', and is 2.5 ± 0.5 . If Sgr A* was located behind Sgr A West, then its flux density would have been attenuated by a factor of 10. However, the spectral index of Sgr A* between 620 MHz and 1.4 GHz is roughly the same as between 1.4 GHz and 8.5 GHz showing no effect of free-free absorption by Sgr A West. This indicates that Sgr A* is located in front of Sgr A West. It is possible to invoke alternate scenarios like sharp enhancement of the 620 MHz flux density of Sgr A* to compensate for the absorption due to Sgr A West or a hole in Sgr A West along the line of sight to Sgr A*, but these appear to be unlikely. In a high resolution radio continuum (resolution $\sim 0.6''$) map (Roberts & Goss 1993), Sgr A* appears to be located slightly ($\sim 1''$) above the junction of the Bar and the Northern arm and diffuse emission can be seen near its position. In radio recombination line (resolution $\sim 2''$) data (Roberts & Goss 1993), emission at the position of Sgr A* is observed near a velocity of 56 km s^{-1} . There is a region of molecular line emission at the outer edge of the Sgr A West, which is known as Circumnuclear Disk (CND), and Roberts & Goss (1993) suggests the recombination line to be stimulated emission from a region near the interior edge of the CND. However, the emission is observed beyond the synthesised half power beam width of Sgr A* and the velocity of emission matches with that of the H 92 α emission from Northern arm. Therefore, it appears that the diffuse gas seen in the radio continuum image near Sgr A* is actually associated with the Northern arm (see also Schwarz et al. (1989)), which indicates that it is located behind Sgr A* (see also Sect. 1). Any hole in this ionised gas has to be smaller than $1''$, which is unlikely. Thus, Sgr A* is located in front of Sgr A West.

5 CONCLUSIONS

Observations of the GC region at 1010, 620 and 580 MHz with the GMRT and a comparison with the existing observations made at other radio frequencies have provided us several important details about the region:

(i) Sgr A* has been detected at 580 MHz, which is the lowest frequency unambiguous detection of Sgr A*, and the estimated flux density is consistent with what is expected from its higher radio frequency spectral index and the flux density. This indicates that there is no low frequency turnover of its emission at frequencies above 0.6

GHz.

(ii) Our observations at 0.6 GHz breaks the degeneracy between emission measure and electron temperature in the existing data, and allows us to estimate the optical depth of the Sgr A West HII region to be about 2.5 at 620 MHz.

(iii) Though Sgr A* is located along the same line of sight as Sgr A West, the emission from it undergoes no absorption by this HII region, which indicates that Sgr A* is located in front of Sgr A West.

ACKNOWLEDGEMENTS

S.R. thanks Miller Goss and Jun Hui Zhao for useful discussions. We also thank Rajaram Nityananda for reading the manuscript and for making useful comments. We thank the staff of the GMRT that made these observations possible. GMRT is run by the National Centre for Radio Astrophysics of the Tata Institute of Fundamental Research. We have used FITS images from the NCSA Astronomy Digital Image Library (ADIL), and the authors wish to thank them.

REFERENCES

- Baars J. W. M., Genzel R., Pauliny-Toth I. I. K., Witzel A., 1977, *A&A*, 61, 99
- Cotton W. D., et al. 1980, *ApJL*, 238, L123
- Davies R. D., Walsh D., Booth R. S., 1976, *MNRAS*, 177, 319
- Ekers R. D., van Gorkom J. H., Schwarz U. J., Goss W. M., 1983, *A&A*, 122, 143
- Falcke H., 1999, in *ASP Conf. Ser.* 186: The Central Parsecs of the Galaxy, pp 113
- Ghez A. M., Klein B. L., Morris M., Becklin E. E., 1998, *ApJ*, 509, 678
- Liszt H. S., van der Hulst J. M., Burton W. B., Ondrechen M. P., 1983, *A&A*, 126, 341
- Lo K. Y., Shen Z., Zhao J., Ho P. T. P., 1998, *ApJL*, 508, L61
- Melia F., Falcke H., 2001, *ARA&A*, 39, 309
- Mezger P. G., Wink J. E., 1986, *A&A*, 157, 252
- Nord M. E., Lazio T. J. W., Kassim N. E., Goss W. M., Duric N., 2004, *ApJL*, 601, L51
- Pedlar A., Anantharamaiah K. R., Ekers R. D., Goss W. M., van Gorkom J. H., Schwarz U. J., Zhao J., 1989, *ApJ*, 342, 769
- Roberts D. A., Goss W. M., 1993, *ApJS*, 86, 133
- Roy S., Rao A. P., 2003, *Astron. Nachr./AN* 324, No. S1, 391
- Roy S., Rao A. P., 2002, in *IAU Symp.* 199: The Universe at low radio frequencies, p 274
- Schwarz U. J., Bregman J. D., van Gorkom J. H., 1989, *A&A*, 215, 33
- Swarup G., Ananthakrishnan S., Kapahi V. K. and Rao A. P., Subrahmanya C. R., Kulkarni V. K., 1991, *Current Science*, 60, 95
- van Langevelde H. J., Frail D. A., Cordes J. M., Diamond P. J., 1992, *ApJ*, 396, 686
- Wakker B. P., Schwarz U. J., 1988, *A&A*, 200, 312
- Whiteoak J. B., Gardner F. F., Pankonin V., 1983, *MNRAS*, 202, 11
- Yuan F., Markoff S., Falcke H., 2002, *A&A*, 383, 854
- Yuan F., Quataert E., Narayan R., 2003, *ApJ*, 598, 301
- Yusef-Zadeh F., 1989, in *IAU Symp.* 136: The Center of the Galaxy, pp 243
- Yusef-Zadeh F., Morris M., Chance D., 1984, *Nature*, 310, 557
- Zhao J., Bower G. C., Goss W. M., 2001, *ApJL*, 547, L29